Fast Evaluation of Advanced Control Structures Based on Rapid Prototyping

Mirela Dobra, Ioan Valentin Sita

Automation Departament, Technical University of Cluj-Napoca

Abstract— Choosing among different control strategies when electric drives with BLDC PM motors are involved, lead inevitably to different heat losses even if the error performances are accepted as similar. Two cases are considered for medium power BLDC PM speed control. First control structure revises the classic P control loop and its practical implementation advantages. The second control algorithm present a modified PID control derived from state space approach. A comparative study based on unconventional infrared thermal imaging is also proposed to evaluate heat losses. Thermal infrared captures are externally made, at the housing level of the BLDC PM motor. When using current and speed feedback, the captured external temperature results higher, in comparison to the case when using only speed as correction signal. A trade off must be established between torque requirements, heat losses and tracking reference signal.Using the Embedded Coder Library and Simulink from Matlab in conjunction to Code Composer Studio, the control algorithms are directly deployed to a real-time developing board, ensuring the premises of the rapid prototyping environment.

Keywords—BLDC PM motor, speed control, PID control, rapid prototyping, thermal analysis.

1. INTRODUCTION

Within the existing work dedicated to Permanent Magnet Synchronous Motor (PMSM) control, many actual studies are concerning with the partial or fully sensorless approaches. In the five past years, a tremendous work was dedicated to digital implementation of the sliding mode observers capable to give a good estimation of the current, speed and position in the electrical drives with PMSM [1]. The major reason the sliding mode was adopted as a good strategy in obtaining good states estimation resides in the similarity between variable structure strategy and the based PWM digital control of electrical drives [2,3]. For electrical drives with medium power PMSM, the fully sensorless trend was also sustained by the continuous improved offer of digital signal controllers on the market [4, 5].

The industrial environment demands, especially the one of CNC routers, are intensively oriented towards replacing the common stepper motors by BLDC PM motors (BrushLess Direct Current with Permanent Magnets). Due to permanent magnet technology providing high efficiency, lower density, smaller size, increased torque, low maintenance, these types of motors qualify the best option on the market even if the implementing costs remain still considerable.

Special interest arises in maintaining the prescribed working conditions. For fast tracking applications like 2D/3D positioning, the speed, position and motion direction must vary rapidly, according to the reference signal. Assuring the specified performances while preserving the operating limitation, these two meet together in the fault detection and isolation approach [6]. Performances in connection to limitations can be also evaluated using qualitative indicators like thermal analysis based on infrared imaging. Used especially for stator construction analysis [7], infrared thermography could be also involved in evaluating between different control loops.

The article presents a quantitative comparison of two speed control loops for electric drives with BLDC PM Motors. The paper main contribution resides in detecting different heat losses for modified PID control loop and classic PI control loop. Beside the measurements accomplished for different speed reference values, it is also established how suitable become the control algorithm in connection to the BLDC PM operating type. Both control structure are also intermediary stages in designing the sliding mode control combined with LMI (Linear Matrix Inequalities) constraints over the current and rotor speed [8].

2. BLDC PM SPEED CONTROL THEORETICAL BACKGROUND

For control algorithm design purposes, the electric drives with BLDC PM motor, in Figure 1 , must be reconsidered to the conventional control model of the transfer function or the state space.

Even if the two mathematical models can cover only the case of linear time invariant systems which is not the case of BLDC PM motors, both approaches give

a good start for further improvements [9]. The typical way [10, 11] of analyzing the behavior of the BLDC PM motor is to model the three voltage phases in the matrix form, relation 1 , also referred as stationary reference frame *abc*:

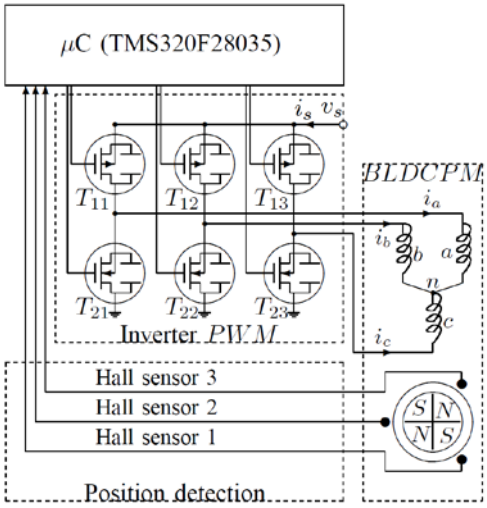

Fig. 1 Schematics of the general electric drive with BLDC PM motor

$$\begin{pmatrix} v_a - v_s \\ v_b - v_s \\ v_c - v_s \end{pmatrix} = R_m^{3\times3}\begin{pmatrix} i_a \\ i_b \\ i_c \end{pmatrix} + L_m^{3\times3}\begin{pmatrix} \frac{di_a}{dt} \\ \frac{di_b}{dt} \\ \frac{di_c}{dt} \end{pmatrix} + K_m^{3\times1}\omega_r \quad (1)$$

with the matrices $R_m^{3\times3}$, $L_m^{3\times3}$ and $K_m^{1\times3}$ constructed as follows: $R_m^{3\times3} = \begin{pmatrix} R_a & 0 & 0 \\ 0 & R_b & 0 \\ 0 & 0 & R_c \end{pmatrix}$, $L_m^{3\times3} = \begin{pmatrix} L_a & 0 & 0 \\ 0 & L_b & 0 \\ 0 & 0 & L_c \end{pmatrix}$, and $K_m^{1\times3} = \begin{pmatrix} K_{e_a} \\ K_{e_b} \\ K_{e_c} \end{pmatrix}$. The notations v_a, v_b, v_c, i_a, i_b, i_c, R and L are referring the phase voltages, the currents, the resistance and inductance respectively. The last component of the sum in eq. 1 represents the back-EMFs which are directly proportional to rotor speed (angular velocity) by the positive factors $K_{e_a}, K_{e_b}, K_{e_c}$. Considering the star connection of the 3 phases, the stator voltage is represented by which is not accessible to direct measurements in practice.

Considering only two active phases at a time (*a* and *b*), the relation 1 can be rewritten by introducing the term v_{AP} as a variable predefined by the inner functionality of the motor:

$$v_a = v_{AP}, v_b = 0, i_b = -i_a, i_c = 0 \quad (2)$$

$$v_{AP} = (R_a + R_b)i_a + (L_a + L_b)\frac{di_a}{dt} + \left(K_{e_a} + K_{e_b}\right)\omega_r \quad (3)$$

The term $v_{AP} = u \cdot v_s$ is introduced as the pulse width modulated voltage supplied to the upper stage of the inverter in Figure 1, with u∈[0,1].

If the same procedure is applied for the two cases of active phases and introducing a convenient average current $\bar{\imath}(t) = \frac{i_s(t)}{u}$, the relation 1 can be reshaped in relation 4 by neglecting the commutation block:

$$v_{AP} = R\bar{\imath}(t) + L\frac{d\bar{\imath}(t)}{dt} + K_e\omega_r(t) \quad (4)$$

whit $\mathrm{R} = \frac{2}{3}(\mathrm{R_a} + \mathrm{R_b} + \mathrm{R_c})$, $\mathrm{L} = \frac{2}{3}(L_a + \mathrm{L_b} + \mathrm{L_c})$, and $\mathrm{K_e} = \frac{2}{3}\left(K_{e_a} + K_{e_b} + K_{e_c}\right)$.

The model for the mechanical part of the electrical drive is obtained in (5) by neglecting the Coulombian frictions. The involved notation K_T refers the torque constant, T_m refers the shaft mechanical torque, *J* is the combined inertia of rotor and load and B refers the combined viscous friction of rotor and load. In the context of equation (4) and (5), the rotor speed control of the BLDC PM motor can be implemented following the same procedure as in the brushed DC motors case.

$$\mathrm{K_T}\bar{\imath}(\mathrm{t}) = \mathrm{T_m}(\mathrm{t}) + \mathrm{J}\frac{\mathrm{d}\omega_\mathrm{r}(\mathrm{t})}{\mathrm{dt}} + \mathrm{B}\omega_\mathrm{r}(\mathrm{t}) \quad (5)$$

The difference consists only in designing the correct commutation block that will assure the control signals (direction and the duty factor of u) when negative feedback from the angular velocity. To validate the proposed approach, simulations using the structure in Figure 2 can be made to verify the velocity control loop.

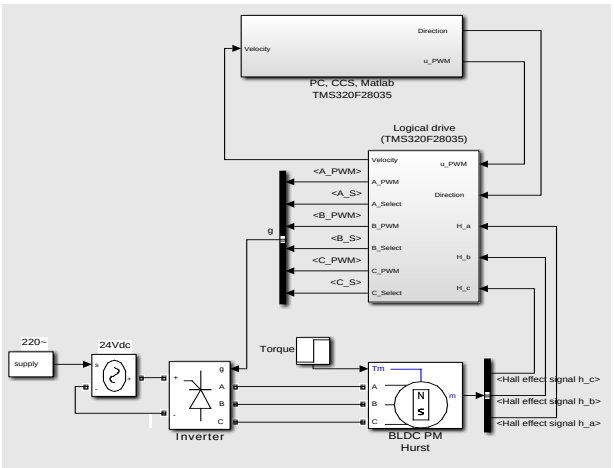

Fig. 2 Matlab / Simulink model for speed control structure simulations

2.1. Simplifying considerations

The BLDC PM motor open loop transfer function resulted by combining (4) and (5) is of second order:

$$H_{ol}(s) = \frac{K_{PWM}K_T}{(Ls+R)(Js+B)+K_TK_e} \quad (6)$$

Based on theoretical observation and datasheet parameters values, further simplifying assumption can be made. The predominant time constants results if comparing the time constant of the electrical subsystem $\frac{R}{L} \simeq \frac{1}{876}$ and the time constant of the mechanical one, $\frac{B}{J} \simeq \frac{1}{3.74\cdot10^4}$. Evaluating also the friction constant and the free term at the denominator of the transfer function, $B \gg K_eK_T$ ($1.19\cdot10^{-2} \gg 4.8\cdot10^{-3}$), results the next convenient simplification:

$$H_{ol}(s) \simeq \frac{K_m}{T_m s+1} \quad (7)$$

where $K_m = \frac{K_{PWM}}{B+K_TK_e}$ and $T_m = \frac{J}{B+K_TK_e}$.

3. MODIFIED PID CONTROL ALGORITHM

The proposed PID algorithm arises from the classic PI speed and current loops. In Figure 3 it is presented the modified block diagram.

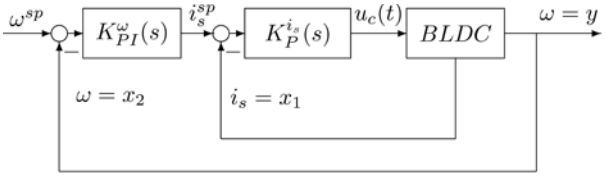

Fig. 3 Block diagram of the modified PID control algorithm

The PID time constants $K_{PID}(s) = k_P + k_I\frac{1}{s} + k_Ds$ can be obtained by rearranging the control signal in the following form, where the internal states are introduced as x_1 and x_2, the stator current and the rotor speed (Figure 3):

$$u_c(t) = k_P^i\left[k_P^{\omega}(\omega^{sp}-x^2) + k_I^{\omega}\int_0^{\infty}(\omega^{sp}-x_2)d\tau - x_1\right]$$
$$= -k_P^i x^1 + k_P^i k_P^{\omega}(\omega^{sp}-x^2) + \cdots \quad (8)$$
$$\ldots + k_P^i k_I^{\omega}\int_0^{\infty}(\omega^{sp}-x_2)d\tau$$

Forcing $x_3(t) = \int_0^{\infty} x_2 d\tau$, as the third internal state, the closed loop with u_c in (5), the state space representation choosing the state rest of variables as physical variables $x = [\,i,\ \omega,\ \int\omega]^T$, results as follows:

$$\frac{dx}{dt} = \begin{pmatrix} -\frac{R}{L} & -\frac{K_e}{L} & 0 \\ \frac{K_T}{J} & -\frac{B}{J} & 0 \\ 0 & -1 & 0 \end{pmatrix}x + \begin{pmatrix} \frac{K_{PWM}}{L} \\ 0 \\ 0 \end{pmatrix}u \quad (9)$$

$$u = \omega^{sp} - K_x x$$
$$y = (0 \quad 1 \quad 0)x$$

If computing K_x as a state reaction vector that places the poles of the closed loop at least two times higer than the open loop ones, the time constant of the PID algorithm results from:

$$K_x = \left(\frac{k_d\ K_T}{J}, \quad k_P - k_d\frac{B}{J}, \quad -k_i\right) \quad (10)$$

Heaving the closed loop in state space representation, the next necessary control enhancement consists in imposing limitation over the current $i_s(t)$ by using linear matrix inequalities (LMI). This potential improvement, by imposing limitation over the current, will be demonstrated as a necessity by making the IR analysis.

4. REDUCED ORDER SLIDING MODE CONTROLLER

Sliding mode control [13] resides in the variable structure control approach. To start the design of the slide surface (line) the convenient mathematical model stands in the state space model. Using (2) and (3), the state space representation for velocity control applications results as:

$$\frac{dx}{dt} = \begin{pmatrix} -\frac{R}{L} & -\frac{K_e}{L} \\ \frac{K_T}{J} & -\frac{B}{J} \end{pmatrix}x + \begin{pmatrix} \frac{K_{AP}}{L} & 0 \\ 0 & -\frac{1}{J} \end{pmatrix}\begin{pmatrix} u \\ v \end{pmatrix}$$
$$y = (0 \quad 1)x$$

where $x(t) = [i(t),\ \ \omega_r(t)]$ stands for the state vector, $u(t)$ the control signal, $y(t)$ the rotor speed and $v(t)$ the uncertainty modelled in additive manner, through the load torque. One approach in designing a reduced order sliding mode control is to introduce a bi-positional relay into the control loop depicted in Figure 4.

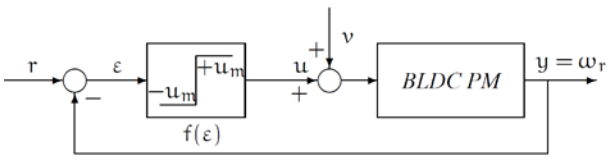

Fig. 4 Negative feedback structure based nonlinearity inside

$$f(\varepsilon) = \begin{cases} u_{max}\ , \varepsilon \geq 0 \\ -u_{max}\ , \varepsilon < 0 \end{cases} \quad (11)$$

The BLDC PM motor transfer function results as $H_{BLDC}(s) = \frac{b_0}{s^2+a_1s+a_0}$ with $a_1 = \frac{R}{L}+\frac{B}{J}, a_0 = \frac{RB+K_eK_t}{LJ}$ and $b_0 = \frac{K_t}{LJ}$. The error signal and its derivatives depending on the output are $\varepsilon(t) = r(t) - \omega(t)$,

$\frac{d\varepsilon(t)}{dt} = -\frac{d\omega(t)}{dt}$, $\frac{d^2\varepsilon(t)}{dt^2} = -\frac{d\omega^2(t)}{dt^2}$. The error equation together with the switching line S of α slope is then given in (12).

$$\frac{d^2\varepsilon(t)}{dt^2} + \frac{a^1 d\varepsilon(t)}{dt} + a_0\varepsilon(t) = a_0 r(t) - b_0 u(t) \quad (12)$$
$$S = \varepsilon(t) - \frac{1}{\alpha}\frac{d\varepsilon(t)}{dt}$$

The command signal u can be then represented as a sign function over the two states of the systems, the current and the velocity [14].

$$u(t) = \begin{cases} u_{max}, \varepsilon(t) - \frac{1}{\alpha}\frac{d\varepsilon(t)}{dt} \geq 0 \\ -u_{max}, \varepsilon(t) - \frac{1}{\alpha}\frac{d\varepsilon(t)}{dt} < 0 \end{cases} \quad (13)$$
$$= sgn(S) \times u_{max}$$

The mathematical condition to sidestep chattering around the switching line is $\frac{d\varepsilon(t)}{dt} = \alpha$. Reducing large chattering in (13) leads to the compact expression of the control law, $u = -(\alpha + 1)\frac{d\varepsilon(t)}{dt}$. To assure the convergence for no chattering conditions, the convenient small adjustment over the control low is applied:

$$u = -(\alpha + 1)\frac{d\varepsilon(t)}{dt} + \delta \cdot \text{sgn}\left[\varepsilon(t) - \frac{1}{\alpha}\frac{d\varepsilon(t)}{dt}\right] \text{ with } \delta > 0 \quad (14)$$

The augmentation over the command signal u can induce closed loop internal instability. The typical way in maintaining the system's stability is to find a Lyapunov function [15] of a convenient form $V(t) = \frac{1}{2}[\varepsilon(t) - \varepsilon(t) - \frac{1}{\alpha}\frac{d\varepsilon(t)}{dt}]^2 = \frac{1}{2}S(e,\dot{e})^2 > 0, \forall e, \dot{e}$. The convenient form is closed related to the energy loss quadratic description. Assessing in relation (14) the first derivative of the Lyapunov function:

$$\dot{V} = S(e,\dot{e}) \cdot \dot{S}(e,\dot{e}) = \frac{\delta}{\alpha} \cdot S(e,\dot{e}) \cdot sgn\big(S(e,\dot{e})\big) > 0 \quad (15)$$
$$\forall e, \dot{e}, \alpha < 0, \delta > 0$$

and having imposed α<0 and δ>0 in (14), the Lyapunov function first derivative remains negative for any $\forall e(t), \dot{e(t)}$. The $V(t)$ negative value represents a necessary and sufficient condition for closed loop stability. When using error convergence based control algorithm like SMC, system's internal stability relies on the powerful Lyapunov test that will assure stable functionality also under modeling errors caused of simplifying considerations [16]

5. EXPERIMENT SETUP

The detailed experiments are parts of the continuous process of upgrading the control structure of the electrical drives viewed as a subsystem of an existing CNC router (2D positioning system). An intermediary stage consists of migrating from the microcontroller F28027 to F28x3x. The two BLDC motors that actuate the ball screw axis, the positioning system is compound of, are of medium power, 5.81oz-in/A. Each of the BLDC PM motors have a nominal speed of 4000 RPM at 24V. To provide access to the angular velocity, the motors are equipped with Hall sensors.

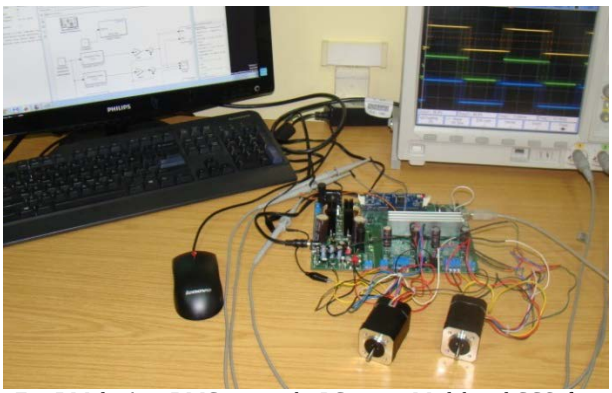

Fig. 5 Multi-Axis DMC next to the PC runing Matlab and CCS, for speed control of BLDC PM motors

The operating system on the PC in Figure 5 is Windows 7. The version of Code Composer Studio is the elder one, V3.3, being the last one that offers software support in conjunction with Matlab Embedded Targets, Release 2013b. Maintaining up to date both the operating system and the adjacent software packages (Code Composer Studio, CCS, and Matlab) is possible by using the new TI products like Multi-Axis DMC.

As a fully functional kit dedicated for sensorless field oriented control for two BLDC PM motor, the specialized kit from Texas Instruments, Multi-Axis DMC (Digital Motor Control), has the advantages of being programmed using the Matlab Embedded Coder that considerably bypass the engineer programing knowledge [6].

The kit integrates two drivers for BLDC PM motors, also produced by Texas instrumentsDRV8402, that are designed as dual full bridge PWM motor driver, operating at up to 500 kHz switching frequency and providing current measurement through external shunt resistor. On the same board of the development kit, it can be attached different control card from TMS320F28x3x family. The tests was made using the Piccolo control card, TMS320F28035, that is a dedicated microcontroller, disposing of enhanced control peripherals like pulse width modulators and capture modules.

6. TEST RESULTS

The case of the modified PID controller and the reduced order sliding mode controller are considered for evaluating the performances of the speed loop with BLDC PM motor.

The two controllers were designed for a motor with the next datasheet parameters: L=4.6mH, R=4.03Ω, J=4.53·10^{-5} kg·m² ,Kt=9.79 ,Ke=0.0691. Imposing a critically damped behavior for the closed loop system, the modified PID algorithm result with the following gains : $k_p = 1.7618, k_i = 594.5767, k_d = 1.4363 \times 10^{-3}$.

Different values of the switching line slope are considered for sliding mode controller, resulting a convenient value $\alpha = -1$.

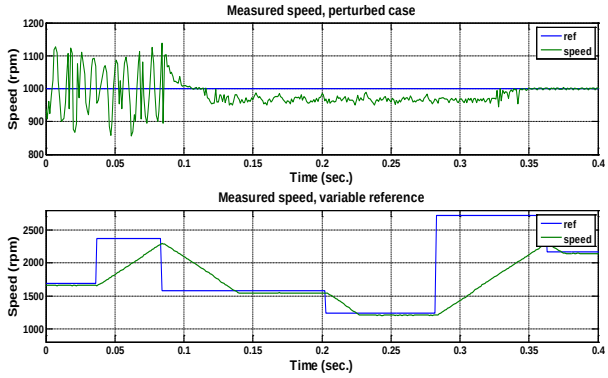

Fig. 6 Modified PID algorithm case

Representative measured speed signals are presented for both cases. In Figure 6, the measured rotor speed when modified PID control and resistive torque is applied on the rotor indicates a larger speed variation than for the case of sliding mode control loop, in Figure 7. When varying the speed reference, in both cases the tracking times are similar. Considering only how well the external torque can be rejected, the sliding mode algorithm shows better performances than the PID one.

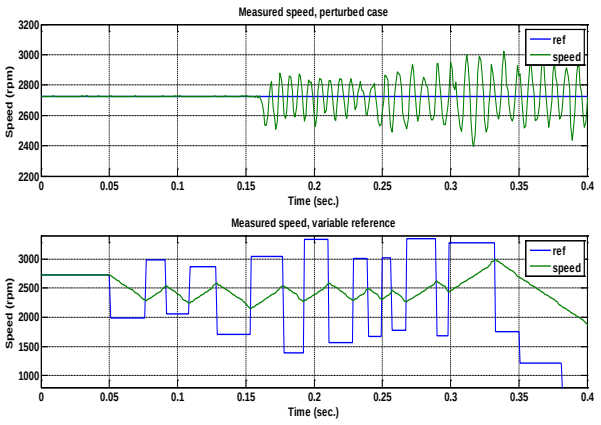

Fig. 7 Sliding mode controller

6.1. Thermal analysis

For analyzing heat losses, it is considered the evaluation of the BLDC PM motor operation at 0.25, 0.4, 0.6 and 0.8 of the nominal speed of 4000rpm. The captured infrared images after 1 hour of no load operation of BLDC PM motor are presented in Table 1 (PID controller) and Table 2 (sliding mode). The infrared images capture the longitudinal position of the motor's housing and the side with the external rotor part (). On every captured image, there are indicated measured spots in Celsius degrees. The measurements were made in laboratory conditions with an ambient temperature around 23^{0}C. Every capture was considered starting from the same initial temperature and at least one hour of pause for the motor.

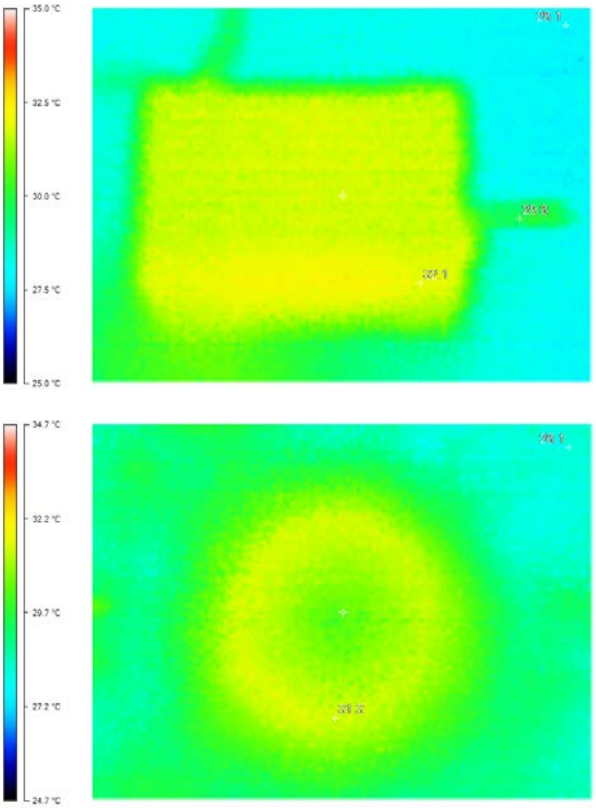

Fig. 8 Captured images for BLDC PM motor in PID control loop, running at 40% of nominal speed

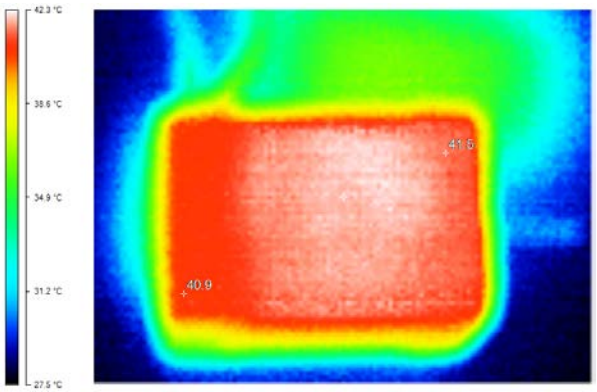

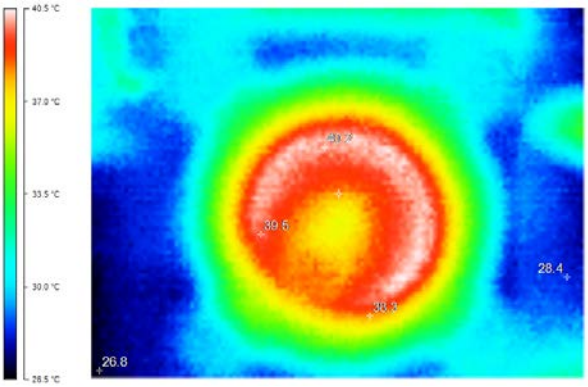

Fig.9 Captured images for BLDC PM motor with sliding mode control, running at 40% of nominal speed

Tabel 1 Table 3 : Celsius degrees spots on motor housing (HT) and rotor (RT) for PID controller and sliding mode based controller (SMC)

Speed (% nominal value)	SMC (HT)	PID controller (HT)	SMC (RT)	PID controller (RT)
25%	40°C	30°C	39°C	29.5°C
40%	41°C	32°C	40°C	31°C
60%	44°C	33.5°C	43.5°C	33°C
80%	46.5°C	36°C	45°C	35.5°C

Evaluating the heat losses for PID controller and SMC cases, expected results of higher heat losses for sliding mode based controller case are obtained.

7. CONCLUSION

The fast setup for speed control loop for electric drives with BLDC PM motor is preponderant in the paper. Without having access to measured speed signal for different control algorithms, thermal analysis become useless.

The temperature measurements demonstrate the necessity of introducing domain constraints for stator current variations that are directly affecting the amount of heat losses.

Starting from the thermal analysis results, further work can be done by connecting the constraints over the current variation to the heat losses. A suitable thermal model can be also derived for the BLDC PM motor operating under mechanical load.

ACKNOWLEDGMENT

The research activities were supported by the project DMI 1.5, ID 137516 -- PARTING, "Inter-university Partnership for Excellence in Engineering", project co-funded from European Social Fund through Sectorial Operational Program Human Resources 2007-2013.

REFERENCES

1. M. Fatu, R. Teodorescu, I. Boldea, G. Andreescu, and F. Blaabjerg, “I-f starting method with smooth transition to emf based motionsensorless vector control of pm synchronous motor/generator,” in Power Electronics Specialists Conference, 2008. PESC 2008. IEEE, June 2008, pp. 1481–1487.
2. V. I. Utkin, “Sliding mode control design principles and applications to electric drives,” Industrial Electronics, IEEE Transactions on, vol. 40, no. 1, pp. 23–36, 1993.
3. Davila, L. Fridman, and A. Levant, “Second-order sliding-mode observer for mechanical systems,” IEEE transactions on automatic control, vol. 50, no. 11, pp. 1785–1789, 2005.
4. ****PiccoloTM Microcontrollers, Data Manual, Texas Instruments, Revised, October 2013. [Online]. Available: http://www.ti.com/lit/ds/symlink/tms320f28035.pdf
5. ****Sensorless Field Oriented Control of Multiple Permanent Magnet Motors, Texas Instruments, June 6, 2010. [Online]. Available: http://www.ti.com/lit/an/sprabq9/sprabq9.pdf
6. R. Isermann, “Process fault detection based on modeling and estimation methodsU° a survey,” Automatica, vol. 20, no. 4, pp. 387–404, 1984.
7. J. Pyrhönen, P. Lindh, M. Polikarpova, E. Kurvinen, and V. Naumanen, “Heat-transfer improvements in an axial-_ux permanentmagnet synchronous machine,” Applied Thermal Engineering, vol. 76, no. 0, pp. 245 – 251, 2015. [Online]. Available: http://www.sciencedirect.com/science/article/pii/S1359431114009910
8. M. Dobra, I. V. Sita, and P. Dobra, “Efficient implementation of sliding mode control for bldc pm motor using tms320f28335 microcontroller,” in Education and Research Conference (EDERC), 2014 6th European Embedded Design in. IEEE, 2014, pp. 70–74.
9. R. Precup, S. Preitl, and P. Korondi, “Fuzzy controllers with maximum sensitivity for servosystems,” Industrial Electronics, IEEE Transactions on, vol. 54, no. 3, pp. 1298–1310, 2007.
10. S. M. Niapour, M. Tabarraie, and M. Feyzi, “A new robust speed-sensorless control strategy for high-performance brushless DC motor drives with reduced torque ripple,” Control Engineering Practice, vol. 24, no. 0, pp. 42 – 54, 2014. [Online]. Available: http://www.sciencedirect.com/science/article/pii/S0967066113002268
11. A. Kapun, M. Èurkoviè, A. Hace, and K. Jezernik, “Identifying dynamic model parameters of a {BLDC} motor,” Simulation Modelling Practice and Theory, vol. 16, no. 9, pp. 1254 – 1265, 2008. [Online]. Available: http://www.sciencedirect.com/science/article/pii/S1569190X08001263
12. ****Motor Control and PFC DeveloperŠs Kit Quick Start Guide, Texas Instruments, October, 2010. [Online]. Available: http://www.ti.com/lit/ml/sprugq1b/sprugq1b.pdf
13. V. I. Utkin, “Survey paper variable structure systems with sliding modes,” IEEE Transactions on Automatic control, vol. 22, no. 2, 1977.
14. J. Ackermann and V. Utkin, “Sliding mode control design based on ackermann’s formula,” IEEE Trans. on Automatic Control, vol. 43,(2), pp. 234–237, 1998.
15. P. Acosta, “Natural surface design for sliding mode control with multiple discontinuous inputs,” Journal of the Franklin Institute, no. 0, pp. –, 2014.[Online]. Available: http://www.sciencedirect.com/science/article/pii/S0016003214001379.
16. X. Yu and O. Kaynak, “Sliding-mode control with soft computing: A survey,” Industrial Electronics, IEEE Transactions on, vol. 56, no. 9, pp. 3275–3285, 2009.

Mirela DOBRA,
Automation Departament , Technical University of Cluj-Napoca
Cluj-Napoca, Romania
Mirela.Trusca@aut.utcluj.ro,